Fall-back time for photo-ionized Cs atoms attached to superfluid 4He nanodroplets

François Coppens, Johannes von Vangerow, Antonio Leal, Manuel Barranco, Nadine Halberstadt, Marcel Mudrich, Martí Pi, Frank Stienkemeier

▶ **To cite this version:**

François Coppens, Johannes von Vangerow, Antonio Leal, Manuel Barranco, Nadine Halberstadt, et al.. Fall-back time for photo-ionized Cs atoms attached to superfluid 4He nanodroplets. The European Physical Journal D : Atomic, molecular, optical and plasma physics, 2019, 73 (5), pp.94. 10.1140/epjd/e2019-90692-0 . hal-02153869

HAL Id: hal-02153869
https://hal.science/hal-02153869

Submitted on 22 Dec 2020

HAL is a multi-disciplinary open access archive for the deposit and dissemination of scientific research documents, whether they are published or not. The documents may come from teaching and research institutions in France or abroad, or from public or private research centers.

L'archive ouverte pluridisciplinaire **HAL**, est destinée au dépôt et à la diffusion de documents scientifiques de niveau recherche, publiés ou non, émanant des établissements d'enseignement et de recherche français ou étrangers, des laboratoires publics ou privés.

EPJ manuscript No.
(will be inserted by the editor)

Fall-back time for photo-ionized Cs atoms attached to superfluid ^{4}He nanodroplets

F. Coppens[1], J. von Vangerow[2], A. Leal[3], M. Barranco[1,3,4], N. Halberstadt[1], M. Mudrich[5], M. Pi[3,4], and F. Stienkemeier[2,6]

[1] Laboratoire des Collisions, Agrégats, Réactivité, IRSAMC, UMR 5589, CNRS et Université Paul Sabatier-Toulouse 3, 118 route de Narbonne, F-31062 Toulouse Cedex 09, France
[2] Physikalisches Institut, Universität Freiburg, 79104 Freiburg, Germany
[3] Departament FQA, Facultat de Física, Universitat de Barcelona. Diagonal 645, 08028 Barcelona, Spain
[4] Institute of Nanoscience and Nanotechnology (IN2UB), Universitat de Barcelona, Barcelona, Spain.
[5] Department of Physics and Astronomy, Aarhus University, 8000 Aarhus C, Denmark
[6] Freiburg Institute of Advanced Studies (FRIAS), University of Freiburg, 79194 Freiburg, Germany

Received: date / Revised version: date

Abstract. We have studied the dynamic evolution of a Cs atom photo-excited from 6s to 6p and 7s states on a helium droplet using time-dependent ^{4}He-DFT simulations. Depending on the excited electronic state, the Cs impurity remains on the droplet surface or it is ejected. Upon subsequent photo-ionization of the excited Cs atom the resulting Cs^+ cation may either be ejected or come back to the droplet, depending on the time delay between photo-excitation and photo-ionization. We have calculated the critical time delay separating these two different behaviors, as well as final ion velocities. These observables will be used for future comparison with planned pump-probe experiments.

PACS. 36.40.-c Atomic and molecular clusters – 78.40.-q Absorption spectra of impurities

1 Introduction

He nanodroplets are often considered the "ideal spectroscopic matrix" owing to their extraordinary properties [1]. Their extremely low intrinsic temperature (0.37 K) leads to efficient cooling of embedded impurities (atoms, molecules, clusters, nanostructures); their chemical inertness makes He nanodroplets a weakly perturbing environment that allows to record highly resolved molecular spectra [2]; due to their superfluid nature, embedded impurities are mobile and readily aggregate into clusters and complexes inside He nanodroplets. However, this concept of a weakly perturbing environment is challenged when impurities are electronically excited or ionized using visible up to extreme ultraviolet radiation [3]. Absorption spectra of droplet-embedded atoms and molecules are often massively blue-shifted and broadened due to Pauli repulsion of the excited orbital from the surrounding helium. This repulsion tends to induce the formation of a void bubble around the excited dopant and even its ejection out of the droplet [4–7].

Alkali (Ak) atoms attached to superfluid helium droplets are known to reside in a dimple at the surface of the droplet, an experimental fact well reproduced by Density Functional Theory (DFT) calculations [8–10]. Electronic excitation of the impurity triggers a rich relaxation dynamics in the Ak@^{4}He$_N$ complex. Owing to the repulsion of the excited electron from the helium droplet, most alkalis dissociate from the droplet under np $\leftarrow$ ns excitation, either as a bare atom or with one or a few atoms attached to it (so-called "exciplexes") [3,11,12]. The heavier ones, Rb and Cs, exhibit a more complex behavior. A Cs atom photo-excited from the 6s to the 6p state or a Rb atom upon 5p $\leftarrow$ 5s excitation can be ejected as a bare atom or as an exciplex, or remain at the droplet surface [13,14].

If the excited cesium atom, here denoted as Cs*, is ejected and it is subsequently photo-ionized, the Cs^+ photo-ion can keep dissociating as a bare cation or as a He_nCs^+ complex, or fall back onto the droplet, eventually sinking into it [15,16]. Whether the cation is ejected or sinks into the droplet interior depends on the delay time τ_D between excitation and ionization. Helium-positive charge interaction is attractive, hence the cation tends to be solvated. This is the case if ionization occurs at short τ_D, when Cs* is still close enough to feel the attraction from the droplet and has not acquired too much kinetic energy. On the other hand, for large τ_D, Cs^+ will keep dissociating because Cs* has already traveled a long distance and acquired a large amount of kinetic energy, so that the attractive He-cation interaction is not strong enough to make it turn around. The critical time τ_c separating both processes has been termed fall-back time [17].

The real-time dynamics of the photo-excitation of Rb atoms to the 5p and 6p states and their subsequent photo-

ionization has been investigated using femtosecond imaging spectroscopy and helium time-dependent density functional theory (He-TDDFT) [18]. It was shown that the desorption dynamics of the Rb* excited atom proceeded on very different time scales depending on the excited state, about ∼1 ps for 6p Rb* and ∼ 100 ps for 5p Rb*. Comparison between theory and experiment indicated that desorption was either impulsive (6p) or in an intermediate regime between impulsive dissociation and complex desorption (5p). These studies have stressed the interpretation of the pump-probe dynamics in terms of competition between the repulsion of the excited Rb atom from the droplet on the one hand, and the attraction of the Rb^+ ion to the droplet on the other [17,18]. The combination of femto-second pump-probe spectroscopy and velocity map imaging has proved crucial to disentangle the process of complex formation, desorption and ion solvation dynamics.

He-TDDFT has naturally become the tool of choice for the analysis of real-time processes involving impurities in helium droplets [7,12,19,20], emerging as a compromise between accuracy and numerical feasibility. The aim of this work is to extend our theoretical study on Rb atoms on ^{4}He droplets [17,18,21], to the next heavier Ak, namely Cs, as both species can be studied within the same approach. In particular, we address here Cs atoms excited to the 6p and 7s states. So far, there is no experimental information available for the photo-excitation of Cs atoms followed by their photo-ionization in order to determine the fall-back time. The present calculations may help guide these experiments.

This work is organized as follows. In Sec. 2 we describe the model employed to address the statics and real-time dynamics of a Cs atom photo-excited on the surface of a He droplet. Results for the two excited states (6p and 7s) studied here are discussed in Sec. 3, and a short summary is presented in Sec. 4.

2 Model

2.1 Statics

We have considered a droplet made of $N = 1000$ helium atoms and have first obtained the structure of the neutral Cs-droplet complex in the ground state. Due to the large mass of cesium compared to that of helium, we describe the Cs atom and its cation as classical particles. As a result, their effect on the statics amounts to an external field acting upon the droplet [21,22].

Within the He-DFT approach at zero temperature (T), the energy of a N atoms helium droplet ^4He_N is written as a functional of the helium particle density including an impurity-helium interaction term

$$E[\Psi] = \int d\mathbf{r} \left\{ \frac{\hbar^2}{2m_{\rm He}} |\nabla\Psi|^2 + \mathcal{E}_c(\rho) \right\} + \int d\mathbf{r}\, \rho(\mathbf{r})\, V_X(|\mathbf{r}_{\rm Cs} - \mathbf{r}|) \,, \quad (1)$$

where $\mathbf{r}_{\rm Cs}$ is the impurity location, $\Psi(\mathbf{r})$ is the effective wave function of the superfluid such that $\rho(\mathbf{r}) = |\Psi(\mathbf{r})|^2$, and the functional $\mathcal{E}_c(\rho)$ contains the interaction term within the Hartree approximation and additional terms describing non-local correlation effects [12]. The $\mathcal{E}_c[\rho]$ functional used in the present work is a modified version of the Orsay-Trento functional [23] able to handle very structured helium configurations such as those expected to appear around fairly attractive impurities [24]. The Cs-He ground state pair potential V_X has been taken from [25].

Upon variation of Eq. (1) one obtains the equation to determine the equilibrium density $\rho_0(\mathbf{r})$ of the droplet and the location of the dopant atom $\mathbf{r}_{\rm Cs_0}$

$$\left\{ -\frac{\hbar^2}{2m_{\rm He}} \nabla^2 + \frac{\delta\mathcal{E}_c}{\delta\rho} + V_X(|\mathbf{r}_{\rm Cs} - \mathbf{r}|) \right\} \Psi_0(\mathbf{r}) = \mu\, \Psi_0(\mathbf{r}) \,, \quad (2)$$

where μ is the chemical potential of the He droplet. Equation (2) has been solved in Cartesian coordinates using the ^{4}He-DFT BCN-TLS computing package [26], see [12, 27] and references therein for additional details. We have used a space-step of 0.4 Å.

A two-dimensional view of the dimple state configuration of the Cs atom can be seen in Fig. 3 of [9]. The Cs atom is located 26.6 Å away from the center of mass of the droplet, whose sharp density radius is 22.2 Å.

Since Cs detachment will be caused by photo-excitation, it is convenient to evaluate the 6p ^{2}P ← 6s ^{2}S and the 7s ^{2}S ← 6s ^{2}S absorption spectra to have a precise idea of the energetics of the process. This was done using the DF sampling method [28] with the He-Cs* 6p Σ and Π and the 7s pair potentials of [29]. In the case of 6p excitation spin-orbit (SO) coupling had to be taken into account. It was assumed to be independent of the He-Cs distance [30,31], its intensity being set to reproduce the spin-orbit splitting of bare Cs in the 6p ^{2}P state, namely 554.0 cm^{-1} [32]. The resulting pair potentials are depicted in the left part of Fig. 1 together with the 6s pair potential. The resulting absorption spectra are shown in Fig. 2. The 6p ← 6s absorption spectrum shown in the top plot is similar to that obtained in [9], which was in good agreement with experiment (see also [15]). The 7s ← 6s absorption spectrum is shown in the bottom plot. It is forbidden in the isolated atom and becomes allowed here because of the symmetry breaking introduced by the helium droplet, as in *e.g.* [19]. It is somewhat blue-shifted, as compared to existing experimental and theoretical information [33,34], see Fig. 2 of [34].

The position of the absorption bands with respect to the corresponding atomic lines can be rationalized by looking at the right part of Fig. 1, which displays the potential energy curves for Cs interacting with a $^4He_{1000}$ droplet with density frozen at that of the ground electronic state equilibrium. All the absorption maxima are blue shifted compared to the atomic lines, as expected from the position of the Franck-Condon region. The largest blue shift is for 7s ← 6s absorption, followed by absorption to the $^2\Sigma_{1/2}$ state of the 6p manifold. In both cases the Cs atom is given a large initial kinetic energy. Absorption to the

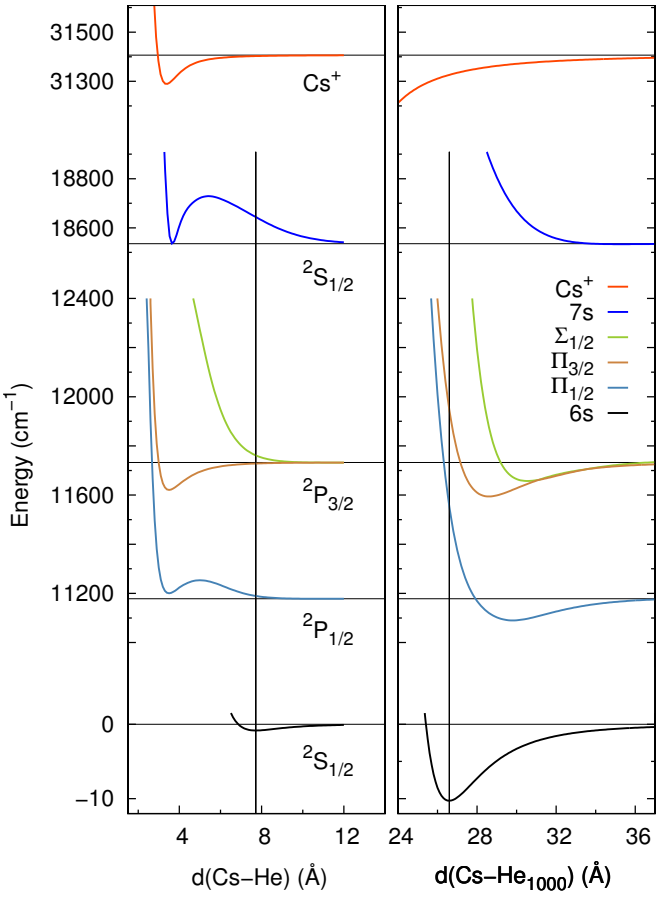

Fig. 1. Left part: He-Cs pair potentials used in this work. Right part: He_{1000} droplet-Cs interaction potentials with the droplet density frozen at its equilibrium value with Cs in its ground electronic state. In both cases a vertical line is drawn from the ground electronic state equilibrium position in order to help visualize the Franck-Condon region.

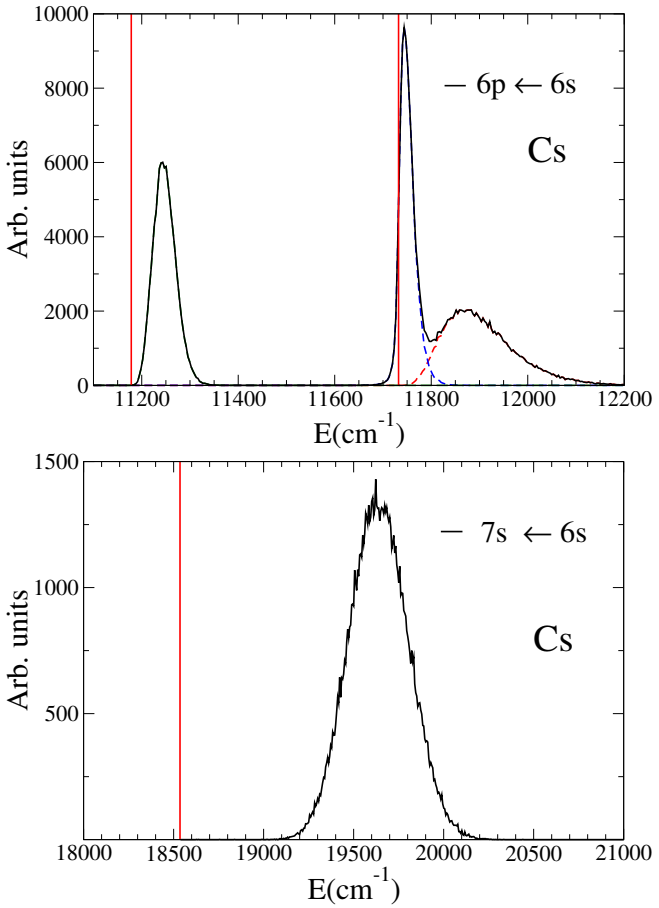

Fig. 2. Top: Dipole absorption spectrum of Cs@^{4}He$_{1000}$ around the 6p ← 6s transition (arbitrary units). The vertical thin lines represent the free Cs atom transitions; the low energy D1 line comes entirely from excitation to the $^2\Pi_{1/2}$ state. The high energy D2 line is decomposed into its $^2\Pi_{3/2}$ (blue dashed line) and $^2\Sigma_{1/2}$ (red dotted line) components. Bottom: same as top for the 7s ← 6s transition.

6p $^2\Pi_{3/2}$ state is rather close to the atomic ^{2}P$_{3/2}$ line, with a small initial kinetic energy given to the Cs atom. Absorption to the 6p $^2\Pi_{1/2}$ state is intermediate, with a non-negligible recoil kinetic energy. These observations already give a hint of what to expect from the photodissociation dynamics on each of these states.

2.2 Dynamics

The simulations presented in this work have been carried out within the He-TDDFT approach [35] briefly outlined here. We introduce a complex effective wave function $\Psi(\mathbf{r},t)$ representing the helium droplet, such that $|\Psi(\mathbf{r},t)|^2 = \rho(\mathbf{r},t)$. It is evolved following the He-TDDFT prescription, while the motion of the excited Cs atom $\mathbf{r}_{Cs^*}(t)$ is treated classically.

In the case of 6p excitation the evolution of the Cs* electronic state has to be also described. To this end, we introduce a six-component normalized vector $|\lambda\rangle$ written in terms of a product basis of spin and angular momentum functions. The electron angular momentum is written in cartesian basis functions $i = x, y, z$ (standing for p_x, p_y and p_z orbitals) and the spin state as $s = \uparrow$ ($m_s = {}^1/_2$), $\downarrow$ ($m_s = -{}^1/_2$)

$$|\lambda\rangle = \sum_{is} \lambda_{is} |i, s\rangle \quad . \tag{3}$$

The complete set of dynamical variables characterizing the system thus consists of a complex effective wave function for helium $\Psi(\mathbf{r},t)$, a vector position for the impurity, $\mathbf{r}_{Cs^*}(t)$, and a 6-dimensional complex vector $|\lambda(t)\rangle$. The total energy of the Cs@^{4}He$_{1000}$ complex suddenly excited to the ^{2}P manifold is written as

$$E[\Psi, \mathbf{r}_{Cs^*}, \lambda] = \int d\mathbf{r}\, \frac{\hbar^2}{2m_{He}} |\nabla\Psi|^2 + \frac{p^2_{Cs^*}}{2m_{Cs}} + \int d\mathbf{r}\, \mathcal{E}_c[\rho] + \langle\lambda|V_{SO}|\lambda\rangle + \int d\mathbf{r}\, \rho(\mathbf{r})\, V_\lambda(\mathbf{r} - \mathbf{r}_{Cs^*}) \; . \tag{4}$$

The $V_\lambda(\mathbf{r}-\mathbf{r}_{\mathrm{Cs}^*})$ potentials are direction-dependent combinations of the Π and Σ potentials [35]

$$V_\lambda(\mathbf{r}) = \langle\lambda|\mathcal{V}(\mathbf{r})|\lambda\rangle = \sum_{ijss'} \lambda^*_{is}\mathcal{V}^{ijss'}(\mathbf{r})\lambda_{js'} \quad , \qquad (5)$$

where the components of the six-dimensional matrix operator $\mathcal{V}$ are [31]

$$\mathcal{V}^{ijss'}(\mathbf{r}) = \left\{V_\Pi(r)\delta_{ij} + [V_\Sigma(r) - V_\Pi(r)]\frac{r_i r_j}{r^2}\right\}\delta_{ss'} \, . \quad (6)$$

The dynamical evolution of the system is obtained by solving the following coupled 3D, time-dependent system

$$\begin{aligned} i\hbar\frac{\partial}{\partial t}\Psi &= \left[-\frac{\hbar^2}{2m_{\mathrm{He}}}\nabla^2 + \frac{\delta\mathcal{E}_c}{\delta\rho} + V_\lambda(\mathbf{r}-\mathbf{r}_{\mathrm{Cs}^*})\right]\Psi \\ i\hbar\frac{\partial}{\partial t}|\lambda\rangle &= \mathcal{H}\,|\lambda\rangle \\ m_{\mathrm{Cs}}\ddot{\mathbf{r}}_{\mathrm{Cs}^*} &= -\int d\mathbf{r}\,[\nabla\rho(\mathbf{r})]V_\lambda(\mathbf{r}-\mathbf{r}_{\mathrm{Cs}^*}) \end{aligned} \qquad (7)$$

The electronic Hamiltonian $\mathcal{H}$ is a 6×6 matrix with elements

$$H^{ijss'} = \int d\mathbf{r}\,\rho(\mathbf{r})\mathcal{V}^{ijss'}(\mathbf{r}-\mathbf{r}_{\mathrm{Cs}^*}) + V_{SO}^{ijss'} \qquad (8)$$

Equations (7) have been solved with the ^{4}He-DFT-BCN-TLS computing package, using a time step of 0.5 fs and the same grid as for the static problem. The initial conditions were chosen to reflect as closely as possible femtosecond pump-probe experimental conditions. In this context the exciting laser pulse is short enough that the nuclei do not have time to move and the excitation process can be described as instantaneous. As a result the initial conditions were taken as: the equilibrium position of Cs at the surface dimple; the associated helium density $\rho_0(\mathbf{r})$ –or effective wave function $\Psi_0(\mathbf{r})$– and atom position $\mathbf{r}_{\mathrm{Cs}^*_0}$ with initial velocity $\dot{\mathbf{r}}_{\mathrm{Cs}^*} = 0$.

Moreover, the energy width associated with pulses of the order of several hundred femtoseconds is of the order of several tens of cm^{-1}, which is small enough to be able to select one initial eigenstate (see right part of Fig. 1). Hence the initial $|\lambda\rangle$ state is taken as one of the eigenstates of the Hamiltonian $\mathcal{H}$ at the time of excitation. Diagonalization of $\mathcal{H}$ yields six eigenstates two-fold degenerate due to Kramer's theorem [36,37]. The dominant term of the electronic Hamiltonian Eq. (8) for Cs* on the helium droplet is the spin-orbit interaction V_{SO}, as was the case for *e.g.* excited Ag atoms [35], Ba$^+$ cations [38] and Rb atoms [21]. Hence the eigenstates can be arranged in two sets depending on their expectation value of $\langle V_{SO}\rangle$: the first set is the doublet correlating to the $J = {}^1/_2$ manifold, and the second set consists of the two doublets (four states) that correlate to the $J = {}^3/_2$ manifold. Evolution corresponding to $^2\Pi_{1/2}$ state excitation was therefore started with $|\lambda\rangle$ equal to one of the eigenstates correlating to the

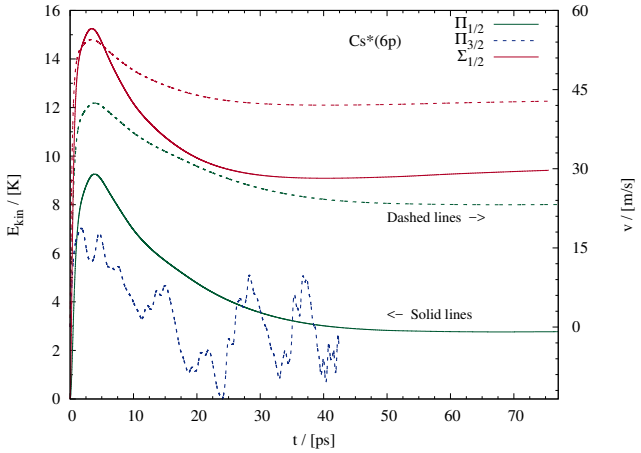

Fig. 3. Velocity (dashed lines, right scale) and kinetic energy (solid lines, left scale) of the Cs atom excited to the 6p state as a function of time. For the $^2\Sigma_{1/2}$ and $^2\Pi_{1/2}$ states the asymptotic velocities would correspond to the largest ion velocities. The kinetic energy of the $^2\Pi_{3/2}$ state is not given as this state is not ejected.

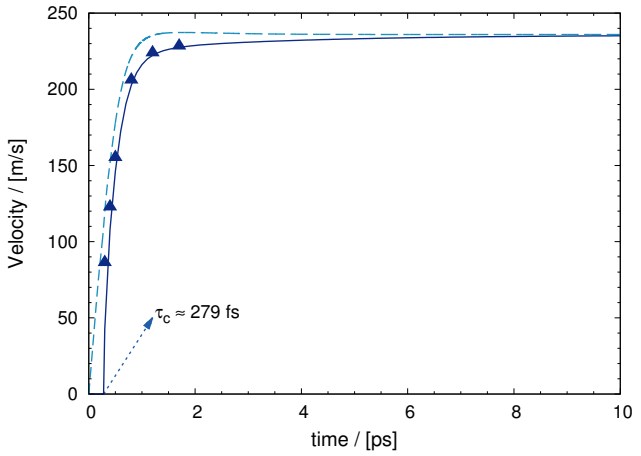

Fig. 4. Dashed line: velocity of the Cs atom excited to the 7s Σ state as a function of time. Solid line: velocity of the Cs$^+$ ion as a function of the delay time obtained from Eq. (14). The triangles are the result of the actual dynamic evolution of the Cs$^+$ cation.

$J = {}^1/_2$ manifold. To select the eigenstate corresponding to $^2\Pi_{3/2}$ or $^2\Sigma_{1/2}$ excitation we have proceeded as follows. Diagonalization of the J_z operator in the fourfold vector space correlating to the $J = {}^3/_2$ manifold results in two doublets with $J_z = \pm{}^3/_2$ or $J_z = \pm{}^1/_2$. Either state of the former doublet was used to start the evolution corresponding to $^2\Pi_{3/2}$ excitation, and either of the latter for $^2\Sigma_{1/2}$ excitation.

Since Cs*(6p) $\rightarrow$ Cs$^+$ ionization is also performed with femtosecond probe pulses, it is described as an instantaneous process: the nuclei do not change position and only the potential electronic surface is suddenly switched to the ionized state at the time of ionization τ_D. The dynamics then proceeds by simulating the time evolution of Cs$^+$ and of the helium density. Since Cs$^+$ is in its ground electronic

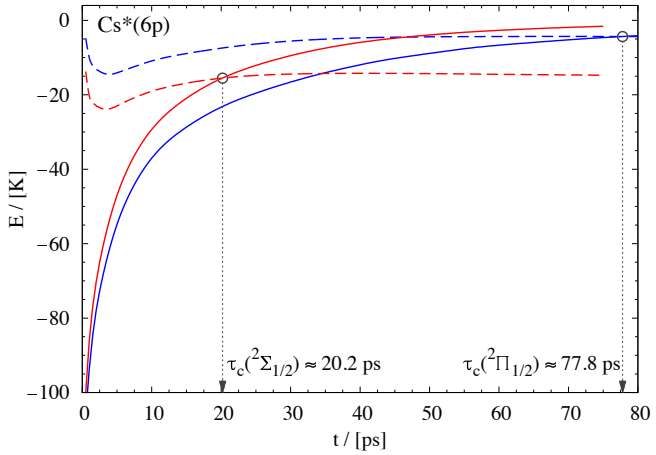

Fig. 5. $U^+(t)$ for Cs in the 6p $^2\Sigma_{1/2}$ and $^2\Pi_{1/2}$ states (solid lines). Also shown are the Cs* kinetic energies of Fig. 3 changed of sign (dashed lines). The intersection of the $U^+(t)$) and $-E_{kin}(t)$ curves corresponding to the same state yields the fall-back time τ_c [Eq. (12)] for that state.

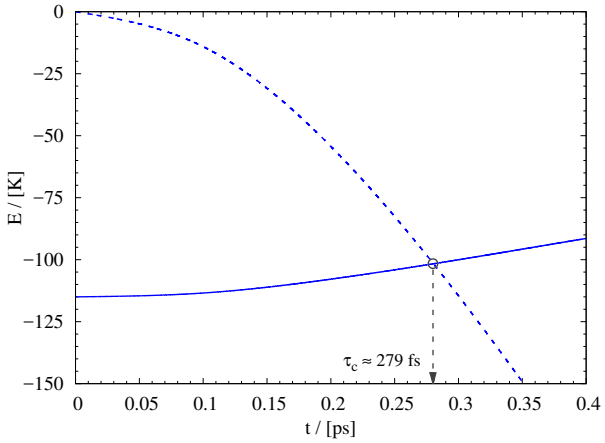

Fig. 6. $U^+(t)$ for Cs in the 7s Σ state (solid line). Also shown is the Cs* kinetic energy changed of sign (dashed line). The intersection of the $U^+(t)$ and -$E_{kin}(t)$ curves yields the fall-back time τ_c [Eq. (12)].

state the equations of motion reduce to

$$i\hbar\frac{\partial}{\partial t}\Psi = \left[-\frac{\hbar^2}{2m_{\rm He}}\nabla^2 + \frac{\delta\mathcal{E}_c}{\delta\rho} + V^+(|\mathbf{r}-\mathbf{r}_{\rm Cs^+}|)\right]\Psi$$
$$m_{\rm Cs}\ddot{\mathbf{r}}_{\rm Cs^+} = -\int d\mathbf{r}[\nabla\rho(\mathbf{r})]V^+(|\mathbf{r}-\mathbf{r}_{\rm Cs^+}|) \qquad (9)$$

with initial conditions for $\mathbf{r}_{\rm Cs^+}$ and $\dot{\mathbf{r}}_{\rm Cs^+}$ given by the corresponding values for the Cs* atom at the delay time, *i.e.* $\mathbf{r}_{\rm Cs^+}(\tau_D) = \mathbf{r}_{\rm Cs^*}(\tau_D)$, $\dot{\mathbf{r}}_{\rm Cs^+}(\tau_D) = \dot{\mathbf{r}}_{\rm Cs^*}(\tau_D)$ while Ψ at τ_D is taken as equal to Ψ for the Cs* dynamics at τ_D. The Cs$^+$-He pair potential has been taken from [16], which sensibly coincides with that of [39]. It is represented as the top curve in the left part of Fig. 1.

Excitation to the 7s state and subsequent ionization are simulated in the same way as for 6p excitation. The sole difference is that the time evolution of Cs* is much simpler, as there is only one electronic state involved in the photo-excitation. Hence Eqs. (7) reduce to

$$i\hbar\frac{\partial}{\partial t}\Psi = \left[-\frac{\hbar^2}{2m_{\rm He}}\nabla^2 + \frac{\delta\mathcal{E}_c}{\delta\rho} + V_{7s}(|\mathbf{r}-\mathbf{r}_{\rm Cs^*}|)\right]\Psi$$
$$m_{\rm Cs}\ddot{\mathbf{r}}_{\rm Cs^*} = -\int d\mathbf{r}\,[\nabla\rho(\mathbf{r})]\,V_{7s}(|\mathbf{r}-\mathbf{r}_{\rm Cs^*}|) \qquad (10)$$

The 7s Cs*-He pair potential has also been taken from [29]. It is represented in the left part of Fig. 1.

3 Results

3.1 Dynamics of Cs* ejection

Figure 3 shows the velocity of Cs* in the center of mass reference system of the Cs@^{4}He$_{1000}$ complex for the three possible excited states corresponding to 6p Cs. Due to the large mass difference between the atom and the droplet, this reference system sensibly coincides with the proper reference system of the helium droplet, where it is at rest. As can be seen in this figure, 6p $^2\Sigma_{1/2}$ and 6p $^2\Pi_{1/2}$ excitation leads to Cs* dissociation. The overshoot in Cs* velocity observed at short times when Cs* dissociates is due to the existence of an attractive well in the excited state potentials. At longer times the Cs* velocity reaches its asymptotic value: 43.6 m/s for 6p $^2\Sigma_{1/2}$ and 23.8 m/s for 6p $^2\Pi_{1/2}$ states. Our result for Cs in the 6p$^2\Pi_{1/2}$ state is not in contradiction with the finding in [15] that Cs excited to this state is not desorbed, as these results correspond to exciting the Cs atom to the low energy tail of the D1 line and ours to the peak energy. A similar situation appeared for Rb* [18,40].

Figure 3 also shows that upon excitation to the 6p $^2\Pi_{3/2}$ state, Cs* is not ejected but remains on the droplet surface and oscillates around some kind of equilibrium position about 1 Å above that of the neutral atom at the dimple.

Notice that the largest velocity of the Cs$^+$ cation obtained by photo-ionization from these states is just the asymptotic velocity displayed for the corresponding Cs* atom. Indeed, photo exciting Cs* away from the droplet yields escaping Cs$^+$ cations whose velocity is little affected by the droplet. Hence, they keep the velocity of Cs* before ionization.

The dynamics of the photoexcited Cs* can be easily understood from the shape of the V_λ potentials defined in Eq. (5). An approximate representation of these potentials as a function of the droplet-Cs* distance is given in Fig. 1. They are obtained by diagonalizing the electronic Hamiltonian of Eq. (8) for a helium density $\rho(\mathbf{r})$ frozen at the ground state equilibrium. The Cs*-He$_{1000}$ interaction potentials corresponding to the 6p $^2\Sigma_{1/2}$ and 6p $^2\Pi_{1/2}$ states are very repulsive in the Franck Condon region, and as a consequence when the Cs atom is excited to either of them it is quickly ejected. At variance, exciting to the 6p $^2\Pi_{3/2}$

state brings the Cs^*He_{1000} system only slightly above the dissociation limit, so that the droplet can easily dissipate the excess energy and the Cs atom remains bound. In addition, as revealed by the corresponding pair potential in the left part of Fig. 1, a He-Cs* excimer can be formed with no barrier. In 3 dimensions there are two deep attractive wells along the symmetry axis of the system, one between the droplet and the Cs* and the other on the other side of the Cs* with respect to the droplet. The former one is rapidly filled by helium atoms due to the absence of a barrier, leading to the formation of a linear exciplex [38]. By visual inspection of the He-TDDFT simulation, we have determined that this exciplex is formed in about 25 ps. The potential well is so deep that, once formed, the exciplex does not detach from the droplet. However, dissociation can occur upon relaxation to the $^2\Pi_{1/2}$ state. This possibility, already identified for 5p Rb* [18], 4p K* [43], or 6p Ba^{+*} [44] is discussed below.

Figure 4 shows the velocity of Cs* upon excitation to the 7s state as a function of time. The calculated maximum velocity of Cs* is 235.9 m/s. In this case, the excited Cs is submitted to a highly repulsive interaction with He (see the corresponding potential curve in the right part of Fig. 1) and is ejected impulsively. This repulsion between He and 7s Cs* also yields a large blue-shift in the absorption spectrum, see the bottom panel of Fig. 2.

3.2 Cs^+ dynamics

Upon ionization at a given time delay τ_D, the Cs^+ ion at $\mathbf{r}_{Cs^+}(t)$ evolves submitted to the potential

$$U^+(\mathbf{r}_{Cs^+}(t)) = \int d\mathbf{r}'\, V^+(|\mathbf{r}_{Cs^+}(t) - \mathbf{r}'|)\, \rho(\mathbf{r}', t) \qquad (11)$$

Notice that $U^+(\mathbf{r}_{Cs^+}(t))$ depends on the state from which Cs* has been photo-ionized (since $\rho(\mathbf{r}, t)$ does).

The fall-back time τ_c has been defined in the introduction as the critical value of the time delay τ_D between excitation and ionization which separates the two possible outcomes for the ion: if $\tau_D > \tau_c$, Cs^+ will keep dissociating, whereas if $\tau_D < \tau_c$, Cs^+ will turn around and get solvated in the helium droplet. Since Cs is treated as a classical particle, the fall-back time τ_c for a given Cs* state is the solution of the equation

$$E_{kin}(\tau_c) + U^+(\tau_c) = 0\,, \qquad (12)$$

where $E_{kin}(t)$ is the kinetic energy of Cs* at time τ_D, which is taken to be equal to the initial kinetic energy for the ion [see text preceding Eq. (9)]. This condition defines the escape point of the ion; if ionization takes place at $\tau_D > \tau_c$, Cs^+ will go away from the system carrying some kinetic energy. The fall-back times for the 6p states are $\tau_c = 20.2$ ps ($^2\Sigma_{1/2}$) and $\tau_c = 77.8$ ps ($^2\Pi_{1/2}$), see Fig. 5. In the case of 7s Cs, we have obtained $\tau_c = 279$ fs, see Fig. 6.

Due to the long range of the ion-He interaction (in $1/r^4$), determining the asymptotic velocity of the ejected ion for a given delay $\tau_D > \tau_c$ is a very cumbersome task, because it requires to simulate the evolution of Cs^+ for hundreds or even thousands picoseconds. This has been done only for a few test cases, as we did for Rb^+ [18]. In general, we have used the method described below, which is accurate and efficient.

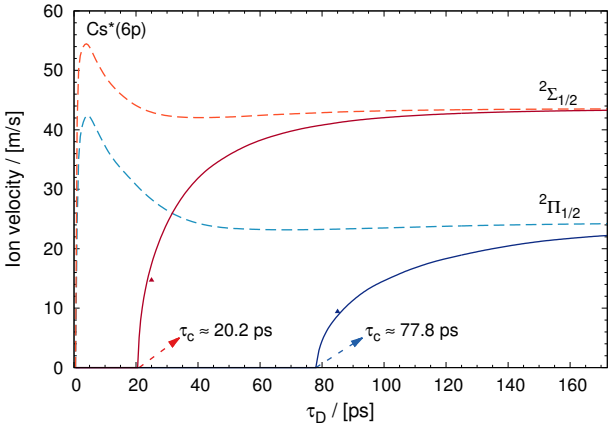

Fig. 7. Velocity of the Cs^+ ion in the $6p^2\Sigma_{1/2}$ and $6p^2\Pi_{1/2}$ states vs. delay (solid lines), and velocity of the neutral Cs* in the corresponding state (dashed lines). The triangles represent the result of two explicit evolutions of the cation in the $6p^2\Sigma_{1/2}$ and $6p^2\Pi_{1/2}$ states for a delay of 25 ps and 85 ps, respectively.

We have followed the actual evolution of the cation from the chosen τ_D up to a rather long time t_{fr} at which the Cs^+ cation is far enough from the droplet that the droplet density can safely be considered as frozen. Energy conservation for the Cs^+ cation gives then its asymptotic energy $[E_{kin}(Cs^+)]_{t_\infty}$ as its total energy at t_{fr}:

$$[E_{kin}(Cs^+) + U(Cs^+)]_{t_{fr}} = [E_{kin}(Cs^+)]_{t_\infty} \qquad (13)$$

Hence, the asymptotic velocity of the ion Cs^+ as a function of the time delay is determined as

$$v_{Cs^+}(\tau_D) = \sqrt{\frac{2}{m_{Cs}}[E_{kin}(Cs^+) + U(Cs^+)]_{t_{fr}}} \qquad (14)$$

Notice that the maximum velocity of the ion obtained from Eq. (14) coincides with the asymptotic velocity of the excited neutral Cs atom, as it should be.

Figure 7 shows the velocity of the Cs^+ ion in the $6p\,^2\Sigma_{1/2}$ and $6p\,^2\Pi_{1/2}$ states as a function of the time delay between excitation and ionization. The velocities of the neutral Cs* atoms are displayed in dashed lines. Also shown in the figure is the result of two actual evolutions of the Cs^+ ion in the $6p\,^2\Sigma_{1/2}$ and $6p\,^2\Pi_{1/2}$ states for a delay of 25 ps and 85 ps, respectively; the results for 7s Cs are shown in Fig. 4. One can see that the agreement of the actual dynamics of Cs^+ with the result obtained from Eq. (14) is good. We have found that the Cs* atom has traveled 11.8 Å before ionization from the $6p\,^2\Sigma_{1/2}$ state, 23.0 Å before ionization from the $6p\,^2\Pi_{1/2}$ state, and 10.2 Å before ionization from the 7s state.

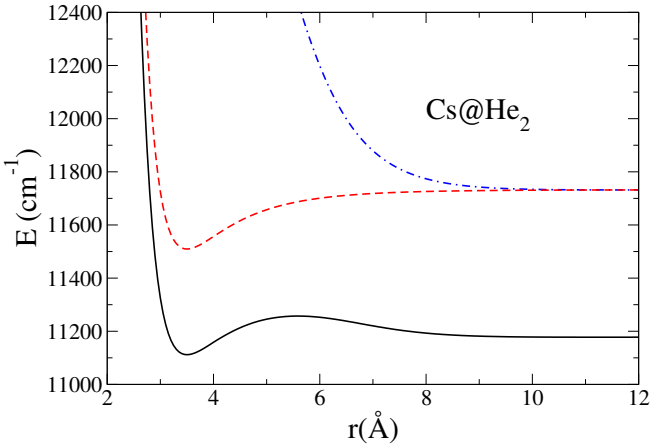

Fig. 8. Energy of the linear symmetric Cs-He$_2$ configuration for Cs* 6p states: $^2\Pi_{3/2}$ (red dashed line), $^2\Pi_{1/2}$ (black solid line), and $^2\Sigma_{1/2}$ (blue dot-dashed line), as a function of the Cs-He distance. The wells in the $^2\Pi_{3/2}$ and $^2\Pi_{1/2}$ curves correspond to the exciplex.

3.3 Role of exciplex formation in the Cs* ejection

As already discussed [see also Fig. 3], Cs excitation to the $^2\Pi_{3/2}$ state yields a linear exciplex, due to the existence of two deep wells in the $V_\lambda(\Pi_{3/2})$ potential [12]. The linear exciplex built on the droplet surface feels a strong attraction by the droplet and remains trapped at its surface. The same has been found for Ag [35], Ba^+ [38], and Rb [18].

This finding seems to be in contradiction with the experiments that observe exciplex formation and desorption at energies in the range where $^2\Pi_{3/2}$ and $^2\Sigma_{1/2}$ states have some overlap. For the Rb($^2\Pi_{3/2}$) excitation [21], the disagreement was solved by adding a model for spin-orbit relaxation of likely broader applicability. We illustrate it as follows in the case of Cs.

The 6p $^2\Pi_{3/2}$ and 6p $^2\Pi_{1/2}$ energy curves of the Cs-He$_2$ linear symmetric exciplex calculated using the method of [38,42] are displayed in Fig. 8 as a function of the He-Cs* distance. No exciplex can be formed around the 6p $^2\Sigma_{1/2}$ state as there is no local minimum in the corresponding pair potential (see Fig. 1). The energy curves in Fig. 8 are similar to the ones found for Rb [21] and consequently, the mechanism for Cs* ejection from the 6p $^2\Pi_{3/2}$ state must be similar. Upon Cs 6p $\Pi_{3/2}$ excitation, the system evolves in time for some tens of picoseconds, during which an exciplex is formed in a barrierless process as shown by Fig. 8. The Cs-He equilibrium position is thus moved from 7.7 Å in the 6s $^2\Sigma_{1/2}$ state of the potential of [25] to 3.5 Å in the 6p $^2\Pi_{3/2}$ exciplex state. Subsequently, the 6p $^2\Pi_{3/2}$ exciplex relaxes non-radiatively to the 6p $^2\Pi_{1/2}$ state with the same equilibrium distance, some 387 cm^{-1} below (see Fig. 8). Part of the available energy is dispersed into the droplet and the rest goes into initial kinetic energy for the exciplex. As a consequence, the exciplex dissociates from the droplet if it receives enough initial kinetic energy to overcome the attraction from the droplet. Unfortunately, our model does not yield how the available energy is shared between the droplet and the impurity. Experimental information on the velocity of Cs$^+$ ions arising from the excitation of Cs to the 6p $^2\Pi_{3/2}$ state is needed to determine this ratio, as in the case of Rb*(5p) [21]. Depending on its value, Cs* in the 6p $\Pi_{1/2}$ state will remain on the droplet surface or be ejected as a bare Cs* atom or as a HeCs* exciplex that will be subsequently photo-ionized.

4 Summary

We have conducted a study of Cs 6p and 7s excitation dynamics on a He_{1000} droplet using He-TDDFT simulations. The dynamics in the (pump) excited states as well as in the (probe) ionic states are determined.

Excitation to the 7s state leads to direct, impulsive dissociation, as expected from the repulsive He-Cs(7s) interaction potential. The same occurs upon excitation to the 6p $^2\Sigma_{1/2}$ state. Excitation to the 6p $^2\Pi_{1/2}$ also leads to Cs* desorption because the Cs* interaction with the droplet is repulsive in the Franck-Condon region for that state. The apparent disagreement with experiment [15] is easily solved by realizing that our simulation corresponds to exciting at the maximum intensity of the $^2\Pi_{1/2}$ absorption peak whereas the non-dissociating Cs* observed by Theisen *et al* [15] was for excitation at the low energy tail of the D1 line. This can be seen in the right part of Fig. 1, where the potential well in the $^2\Pi_{1/2}$ state can be accessed if the Franck-Condon region extends to about 0.5 Å further from the ground state equilibrium distance, which is very plausible. Finally, excitation to the 6p $^2\Pi_{3/2}$ state leads to barrierless formation of an exciplex which remains bound to the droplet. Eventually spin-orbit relaxation is expected to take place, as surmised and modeled in Rb* 5p $^2\Pi_{3/2}$ [21]. As a consequence, Cs* will dissociate, either as a bare atom or as an exciplex.

We have also simulated the dynamics in the ionic state corresponding to the probe process as a function of the delay time between excitation and ionization. This way the critical time delay τ_c separating ion escape from ion turn back and solvation could be determined. This could be tested against planned experiments.

This work has been performed under Grant No FIS2017-87801-P (AEI/FEDER, UE). MB thanks the Université Fédérale Toulouse Midi-Pyrénées for financial support throughout the "Chaires d'Attractivité 2014" Programme IMDYNHE. JvV, MM, and FS acknowledge support by the Deutsche Forschungsgemeinschaft (MU 2347/6-1 and IRTG 2079). High performance computing resources from CALMIP (Grant P1039) is gratefully acknowledged.

5 Authors contributions

Most calculations were carried out by F. Coppens, A. Leal, and M. Pi. J. von Vangerow carried out experiments on

Rb that have motivated this work and clarified basic aspects of the problem. All the authors were involved in the discussions leading to the completion of this work and the preparation of the manuscript, that was mainly written by M. Barranco, N. Halberstadt, M. Mudrich, and F. Stienkemeier. All the authors have read and approved the final manuscript.

References

1. J. P. Toennies and A. F. Vilesov, Angew. Chem. Int. Ed. **43**, (2004) 2622.
2. F. Stienkemeier and K. Lehmann, J. Phys. B. **39**, (2006) R127.
3. M. Mudrich and F. Stienkemeier, Int. Rev. Phys. Chem. **33**, (2014) 301.
4. E. Loginov and M. Drabbels, J. Phys. Chem. A, **111**, (2007) 7504–7515.
5. X. Zhang and M. Drabbels, J. Chem. Phys., **137**, (2012) 051102
6. N. B. Brauer, S. Smolarek, E. Loginov, D. Mateo, A. Hernando, M. Pi, M. Barranco, W. J. Buma, and M. Drabbels, Phys. Rev. Lett., **111**, (2013) 153002
7. B. Thaler, S. Ranftl, P. Heim, S. Cesnik, L. Treiber, R. Meyer, A.W. Hauser, W.E. Ernst, and M. Koch, Nature Comm. **9**, (2018) 4006.
8. F. Stienkemeier and J. Higgins and C. Callegari and S. I. Kanorsky and W. E. Ernst and G. Scoles, Z. Phys. D **38**, (1996) 253.
9. O. Bünermann, G. Droppelmann, A. Hernando, R. Mayol, and F. Stienkemeier, J. Phys. Chem A **111**, (2007) 12684.
10. A. Pifrader, O. Allard, G. Auböck, C. Callegari, W.E. Ernst, R. Huber, and F. Ancilotto, J. Chem. Phys. **133**, (2010) 164502.
11. C. Callegari and W. E. Ernst, in *Handbook of High Resolution Spectroscopy*, Vol. 3, M. Quack and F. Merkt Eds. (Wiley, New York, 2011), p. 1551.
12. F. Ancilotto, M. Barranco, F. Coppens, J. Eloranta, N. Halberstadt, A. Hernando, D. Mateo, and M. Pi, Int. Rev. Phys. Chem. **36**, (2017) 621.
13. F. Lackner, G. Krois, M. Theisen, M. Koch, and W. E. Ernst, Phys. Chem. Chem. Phys. **13**, (2011) 18781.
14. F. R. Brühl, R. A. Trasca, and W. E. Ernst, J. Chem. Phys. **115**, (2001) 10220.
15. M. Theisen, F. Lackner, and W.E. Ernst, J. Chem. Phys. **135**, (2011) 074306.
16. A. Leal, D. Mateo, A. Hernando, M. Pi, M. Barranco, A. Ponti, F. Cargnoni, and M. Drabbels, Phys. Rev. B **90**, (2014) 224518.
17. J. von Vangerow, O. John, F. Stienkemeier, and M. Mudrich, J. Chem. Phys. **143**, (2015) 034302.
18. J. von Vangerow, F. Coppens, A. Leal, M. Pi, M. Barranco, N. Halberstadt, F. Stienkemeier, and M. Mudrich, J. Phys. Chem. Lett. **8**, (2017) 307.
19. A. Hernando, M. Barranco, M. Pi, E. Loginov, M. Langlet, and M. Drabbels, Phys. Chem. Chem. Phys. **14**, (2012) 3996.
20. A. Vilà, M. González, and R. Mayol, Phys. Chem. Chem. Phys. **18**, (2016) 2006.
21. F. Coppens, J. von Vangerow, M. Barranco, N. Halberstadt, F. Stienkemeier, M. Pi, and M. Mudrich, Phys. Chem. Chem. Phys. **20**, (2018) 9309.
22. F. Ancilotto, E. Cheng, M.W. Cole, and F. Toigo, Z. Phys. D **98**, (1995) 323.
23. F. Dalfovo, A. Lastri, L. Pricaupenko, S. Stringari, and J. Treiner, Phys. Rev. B **52**, (1995) 1193.
24. F. Ancilotto, M. Barranco, F. Caupin, R. Mayol, and M. Pi, Phys. Rev. B **72**, (2005) 214522.
25. S.H. Patil, J. Chem. Phys. **94**, (1991) 8089.
26. 4He-DFT BCN-TLS: A Computer Package for Simulating Structural Properties and Dynamics of Doped Liquid Helium-4 Systems. M. Pi, F. Ancilotto, F. Coppens, N. Halberstadt, A. Hernando, A. Leal, D. Mateo, R. Mayol, and M. Barranco, https://github.com/bcntls2016/
27. M. Barranco, F. Coppens, N. Halberstadt, A. Hernando, A. Leal, D. Mateo, R. Mayol, and M. Pi, *Zero temperature DFT and TDDFT for ^{4}He: A short guide for practitioners* (2017), https://github.com/bcntls2016/DFT-Guide/blob/master/dft-guide.pdf
28. D. Mateo, A. Hernando, M. Barranco, R. Mayol, and M. Pi, Phys. Rev. B **83**, (2011) 174505.
29. J. Pascale, Phys. Rev. A **28**, (1983) 632.
30. J.L. Persson, Q. Hui, Z.J. Jakubek, M. Nakamura, and M. Takami, Phys. Rev. Lett. **76**, (1996) 1501.
31. A. Hernando, M. Barranco, R. Mayol, M. Pi, and M. Krośnicki, Phys. Rev. B **77**, (2008) 024513.
32. A. Kramida, Y. Ralchenko, J. Reader, and NIST ASD Team (2012), NIST Atomic Spectra Database (version 5.0). Available at http://physics.nist.gov/asd. National Institute of Standards and Technology, Gaithersburg, MD.
33. C. Callegari and F. Ancilotto, J. Phys. Chem. A 115 (2011) 6789.
34. J. von Vangerow, A. Stieg, F. Stienkemeier, M. Mudrich, A. Leal, D. Mateo, A. Hernando, M. Barranco, and M. Pi, J. Phys. Chem. A **118**, (2014) 6604.
35. D. Mateo, A. Hernando, M. Barranco, E. Loginov, M. Drabbels, and M. Pi, Phys. Chem. Chem. Phys. **15**, (2013) 18388.
36. A. Nakayama and K. Yamashita, J. Chem. Phys. **114**, (2001) 780.
37. P.H.E. Meier and E. Bauer, *Group Theory* (North-Holland, Amsterdam, 1962).
38. A. Leal, X. Zhang, M. Barranco, F. Cargnoni, A. Hernando, D. Mateo, M. Mella, M. Drabbels, and M. Pi, J. Chem. Phys, **144**, (2016) 094302.
39. A.D. Koutselos, E.A. Mason, and L.A. Viehland, J. Chem. Phys. **93**, (1990) 7125.
40. G. Auböck, J. Nagl, C. Callegari, and W.E. Ernst, Phys. Rev. Lett. **101**, (2008) 035301.
41. G. Droppelmann, O. Bünermann, C.P. Schulz, and S. Stienkemeier, Phys. Rev. Lett. **93**, (2004) 023402.
42. P. Moroshkin, A. Hofer, and A. Weis, Phys. Rep. **469**, (2008) 1.
43. M. Martinez, F. Coppens, M. Barranco, N. Halberstadt, and M. Pi, Phys. Chem. Chem. Phys. **21**, (2019) 3626.
44. P. Vindel Zandbergen, M. Barranco, F. Cargnoni, M. Drabbels, M. Pi, and N. Halberstadt, J. Chem. Phys. **148**, (2018) 144302.
45. L. Fechner and B. Grüner and A. Sieg and C. Callegari and F. Ancilotto and F. Stienkemeier and M. Mudrich, Phys. Chem. Chem. Phys., **14**, (2012) 3843.
46. A. Kautsch and M. Koch and W. E. Ernst, J. Phys. Chem. A, **117**, (2013) 9621–9625.
47. M. Koch and G. Auböck and C. Callegari and W. E. Ernst, Phys. Rev. Lett., **103**, (2009) 035302.